Efficient plasma-catalysis coupling for CH4 and CO2 transformation in a fluidized bed reactor: Comparison with a fixed bed reactor

Nassim Bouchoul, Houcine Touati, Elodie Fourre, Jean-Marc Clacens, Catherine Batiot-Dupeyrat

Efficient plasma-catalysis coupling for CH_4 and CO_2 transformation in a fluidized bed reactor: comparison with a fixed bed reactor

Nassim Bouchoul, Houcine Touati, Elodie Fourré, Jean-Marc Clacens, Catherine Batiot-Dupeyrat*

IC2MP, ENSIP, Université de Poitiers - UMR CNRS 7285
1 rue Marcel Doré, TSA 41105, 86073 Poitiers cedex 9 (France)

*E-mail : catherine.batiot.dupeyrat@univ-poitiers.fr

Abstract

The transformation of methane and carbon dioxide by coupling plasma and catalysis was investigated using a fluidized bed reactor and the results, in terms of reactant conversion and yields in products, were compared with those obtained in a fixed bed reactor. A series of alumina, including a commercial sample and various meso-macro materials synthesized in the laboratory, was tested in this study. Their surface areas varied from 260 to 312 $m^2 g^{-1}$ depending on their calcination temperature. A correlation between reactant conversion and surface area of alumina was highlighted for the plasma-fluidized bed, the best conversions being reached with the alumina presenting the highest surface area. CH_4 conversion increased from 8.5 to 12.1 % for S=260 and 312 $m^2 g^{-1}$ respectively and the CO_2 conversion from 3.4 to 6.2 % for a deposited power of 4W, in an excess of CO_2. This correlation was not corroborated for the fixed bed reactor. It proves that an efficient coupling of plasma and catalysis can be expected as soon as solid particle are moving in the gas flow, enhancing the plasma-surface interaction.

Keywords

CH_4 and CO_2, Non-thermal plasma, fluidized bed, plasma - catalyst interaction, alumina

1 Introduction

The need to develop renewable energy sources in order to reduce greenhouse gas emission is a major contemporary concern, leading to a continuous increase of research activities. To this end, methane and carbon dioxide, the two main constituent of biogas, are particularly studied since the reaction between them (dry reforming) lead to the formation of syngas (H_2 + CO), an important raw material in liquid fuel processes such as Fischer-Tropsch synthesis and methanol synthesis. However, the reaction presents two serious problems: it is very endothermic, requiring temperatures above 700°C and the catalysts deactivate rapidly due to carbon deposition [1]. Consequently, new methods of activation are still needed to perform the reaction in conditions reaching today's economic and environmental constraints.

Non-thermal plasma (NTP) has been the subject of a large array of publications showing that atmospheric pressure and low-temperature plasmas offer an interesting alternative to conventional catalytic thermal processes in the dry reforming reaction [2-6]. Different types of NTP were investigated, the most common being microwave [7], gliding arc discharges [8, 9] and Dielectric Barrier Discharges (DBDs) [10]. DBD reactors present the advantages of operating at atmospheric pressure with a simple design suitable for upscaling. The strong electric field generated by the application of a high voltage (several kV) between two electrodes (one of which being protected by a dielectric material) leads to the formation of highly energetic electrons. These electrons collide with surrounding gas molecules, creating reactive species such as ions, excited species and radicals.

Many reactions occur under non-thermal plasma, leading to valuable products such as hydrocarbons [6] or oxygenates [11] but a poor selectivity towards the targeted products is often referenced. A way to promote the efficiency of the process is to combine plasma with catalysis [12]. However, some antagonist effects were reported. If the interaction between the gas discharge and the surface of the catalyst may lead, in some cases, to significant improvement

when compared to pure plasma system [13], in other cases, lower performances were described. For example, the presence of a reduced Ni/Al_2O_3 catalyst [14] or a zeolite A [15] in the plasma discharge decreased CH_4 and CO_2 conversion. It was suggested that the insertion of a solid in the plasma zone modifies significantly the propagation of the discharge. A shift of the discharge mode from filamentary to a combination of surface discharges, in addition to spatially limited micro-discharges at the contact point of the catalyst pellets were observed [16]. Moreover, the presence of conductive Ni sites decreased the electric field strength and consequently the electron density, reducing reactants conversion [17].

Looking at the catalyst grain size effect, the highest reaction conversions were reached when using the smallest grain size, which was partly attributed to a maximum number of contact points [18, 19]. The main conclusion deriving from the studies combining non-thermal plasma and catalysis would suggest that the volume of gas in the plasma zone is too low to efficiently perform the reactants activation.

The purpose of this paper is to examine the combination of plasma and catalysis in a fluidized bed, considering that the contact between the external surface of grains and plasma discharge can be improved when compared to a fixed bed reactor. Fluidized bed plasmas have been used for pre-treatment of catalysts, under reduced pressure [20] and at atmospheric pressure [21-23] for catalyst surface modification. Wang *et al.* [24] reported the dry reforming of methane in an atmospheric pressure plasma fluidized bed with Ni/Al_2O_3. The authors investigated the reaction at temperatures varying from 648 to 798 K and showed a clear positive effect of the plasma fluidized bed compared to plasma packed bed. Currently, more insight on the understanding of plasma - catalysis interactions in a fluidized bed is needed and particularly on the influence of the materials textural properties on CH_4 and CO_2 reactivities. For that purpose, the study of a series of alumina materials possessing surface areas from 65 $m^2\ g^{-1}$ to 312 $m^2\ g^{-1}$ was achieved in this work. Alumina was chosen due to its low dielectric constant (9-30), favorable to plasma

–catalysis coupling [25]. Indeed, we show in a previous paper that CH_4 and CO_2 conversions can be correlated with the dielectric constant of the material, the lower the dielectric constant, the higher the conversions for both CO_2 and CH_4 [26].

The goals defined here are to determine the influence of 1- the type of reactor (fixed bed versus fluidized bed) and 2- the textural and structural properties of alumina on the CH_4 and CO_2 reactivities.

2 Experimental part

2.1 Experimental setup

The reaction was performed at room temperature and atmospheric pressure under a mixture of helium, methane and carbon dioxide at a total flow rate of 40 mL min^{-1} using a CO_2/CH_4 ratio of 2, with a constant concentration in He: 75%. All the experiments were performed twice with a good accuracy of the measurements within an error of 5%.

The two plasma reactors are described below:

1) Fixed bed plasma: a coaxial dielectric barrier discharges (DBD) reactor (figure 1a). The non-thermal plasma reactor (dielectric barrier discharge) consists in an alumina tube (ID: 4mm; ED: 6mm), a stainless steel electrode centered inside the reactor (1.0mm) and a copper electrode wrapped around the alumina tube (10 cm long). It corresponds to a volume of plasma equal to 1.2 cm^3.
2) Fluidized bed reactor (figure 1b): A fritted glass (2 mm) was inserted in a quartz tube to support the sieved catalyst and favor the fluidization of the catalyst. The reactor possesses an inner diameter of 9 mm and the inner electrode was 3.8 mm in diameter. The external electrode length was chosen in order to obtain the same plasma volume (1.2 cm^3) as for the fixed bed reactor, so the length of the outer electrode was 2.2 cm.

The gas flow, sent from the bottom, was fixed at 40 mL min^{-1}. The catalyst grains remained static on the fritted glass (figure 1b: without plasma). A point to be highlighted is that, the minimum gas flow to reach fluidization is 300mL/min, corresponding to an experimental minimum fluidization velocity of 0.23m.s^{-1}. The theoretical minimum fluidization velocity was also calculated by the Ergun's equation [27] and the simplified formula for Reynolds number proposed by Wen and Yu [28]. A value of Um = 0.29 m.s^{-1} was obtained, not too far from the experimental value.

As soon as the plasma discharge is generated into the reactor, at a low flow of 40 mL.min^{-1}, it is remarkable to observe that fluidization occurs, which can be explained by the presence of electrostatic charges under plasma. The particles move into the reactor with up/down and left/ right movements. (figure 1b: with plasma). Similar observation was reported by Currier et al. using a radio-frequency generator at low pressure (100-500 mTorr) [29]. The authors showed a much higher particle density (SiO_2) in the plasma fluidized bed compared to the experiment without plasma at the same gas-flow rate. They explained that it could result from the interaction of the highly charged particles and the electric and magnetic fields and also to a significant change in the physical properties of the fluidizing agent.

A sinusoidal supply of power was applied across the electrodes (TG1010A Aim-TTi, Thurlby Thandar Instruments Brand). The discharge power, calculated from the Lissajous figures, was fixed at 4 W, keeping the frequency constant at 800 Hz while the voltage was adjusted to keep the deposited power constant. The electrical signals were monitored with high voltage probes (PMK, model PHV4-2757) connected to an oscilloscope (waveRunner 62 Xi, Lecroy). A low power was chosen in order to avoid a thermal effect, which could be caused by joule effect. In that case, the reaction in the reactor remained close to room temperature.

2.2 Gamma alumina

A commercial γ-Al_2O_3 provided by Alfa Aesar was tested. The mesoporous alumina was prepared according to the following procedure, inspired by Z-Y. Yuan et al. [30]: 20.5 g of cetyltrimethylammonium bromide (CTMABr) (purity > 96 %, Sigma-Aldrich) were dissolved in 93.93 g of deionized water. The suspension was stirred at 40 °C for about 1 h, before the addition, under stirring, of 24.12 g of aluminium isopropoxide (Sigma-Aldrich). The resulting sol was further matured under stirring for 3 h. It was then autoclaved under static conditions in a polypropylene bottle at 80°C for 24h. The bottle was cooled to room temperature and the suspension was filtered. The obtained paste was washed 3 times with 200 mL of water. The washed paste was dried at 100 °C overnight. The solids were calcined at three different temperatures: 400, 600 and 800 °C in order to vary the surface area as shown in table 1.

The solids were characterized before and after plasma treatments. Surface areas were measured according to the BET procedure. The nitrogen adsorption-desorption isotherms were determined with a Micromeritics Flowsorb II 2300 appartus at -196°C. Thermogravimetric analysis were performed with a TA Intruments SDT-Q600 analyzer under a 100 mL/min flow of air up to 900°C.

2.3 Gas phase analysis and calculation

The gas phase was analyzed on-line by gas chromatography equipped with FID (oxygenated products) and TCD detectors (hydrogen, carbon monoxide, carbon dioxide, methane). The reaction was performed during one hour.

All the experiments were performed three times after cleaning the inner electrode and changing the catalyst (when used), a margin error of ± 3 % was calculated.

The conversion, selectivity, yields and energy efficiency were defined as:

Conversion (%) of CH_4 and CO_2 = 100 × mole of CH_4 (or CO_2) converted/ mole of CH_4 (or CO_2) in the feed (1)

The selectivity was calculated based on carbon atoms:

Selectivity to C_nH_y (%) = 100 × n × mole of C_nH_y / (mole of CH_4 converted + mole of CO_2 converted) (2)

Selectivity to CO (%) = 100 × mole of CO / (mole of CH_4 + mole of CO_2) converted

Yield in H_2 (%) = 100 × mole of H_2 / 2 x (mole of CH_4) introduced (3)

Carbon Balance: CB (%) = 100 × (mole of CO +$\sum$ n × mole of C_nH_y) / (mole of CH_4 converted + mole of CO_2 converted) (4)

Energy Efficiency: EE (mmol kJ^{-1}) = total mol of CH_4 + CO_2 converted (mmol min^{-1}) / input power (kJ min^{-1}) (5)

3 Results and discussion

3.1 Influence of the geometry of the reactor on the plasma discharge

The geometry of the two reactors (fixed and fluidized bed) differs strongly since a larger gap is required to obtain a fluidized bed and a quartz tube was used as dielectric material to visualize the catalyst in motion. The first experiments were performed in presence of quartz wool in the plasma zone, without catalyst. A constant flow rate of 40 mL min^{-1} was kept through all the experimentations with the same gas composition: He/CO_2/CH_4: 75/17/8%. The deposited power was fixed at 4W.

The influence of the reactor geometry on the reactant conversion is a known effect, described by different authors. It is admitted in the literature that, at constant input power, the larger the electrode gap distance, the weaker the electric field strength [31], a lower reactant conversion being thus expected. However, for the two reactors defined in this study, the results in terms of CH_4 and CO_2 conversions, reported in fig. 2, show that methane conversions are similar, closed

to 9%, while CO_2 conversion in the fixed bed is slightly higher than in the fluidized bed reactor. Such behavior is a consequence of two concomitant effects. First, the gap distance reduction, which increases the plasma energy. The second effect results from the electrode length modification. When the electrode length is increased, the plasma energy lost as heat increases. Indeed, Nozaki et al. [32] showed that 60% of input power was dissipated as heat to the dielectric barrier due to the formation of surface discharge in a DBD reactor fed with methane. For this study, those two effects are counteracting each other, leading to similar methane conversion despite the different gap distances. The higher conversion of CO_2 is followed by a higher yield of CO, while the formation of hydrocarbons is not favored, due to a CO_2/CH_4 ratio higher than unity. Under these experimental conditions, it appears that the residence time, identical and close to 1.1 s for both reactors, is the key parameter on which depends the conversions and this independently of the reactor geometry. The effect of residence time was reported in different studies, at atmospheric pressure, increasing the residence time leads to an increase of reactants conversions [33, 34], while in low pressure system, Uner and Thimsen [35] showed little effect of residence time for CO2 transformation due to fast reaction rate (approximately 1000 times shorter than in atmospheric pressure DBD). The higher CO_2 conversion in the fixed reactor could be due to the presence of alumina as dielectric material. Mora et al. [36] described a better performance for CO_2 hydrogenation with alumina instead of quartz. This effect was attributed to the higher relative dielectric permittivity coefficient of alumina compared to quartz. Additionally, in the dry reforming of methane, higher yield in CO and higher energy efficiency were obtained by Khoja et al. [37] in an alumina reactor compared to a quartz one, which is in agreement with this study.

In presence of a catalyst, the experimental conditions were significantly different for the two reactors. About one gram of alumina powder was necessary to fill completely the plasma zone of the fixed bed while 150 mg of material were required for the fluidized bed.

Lissajous figures of the discharge for the fixed and fluidized bed reactors packed with alumina pellets (γ Al_2O_3 calcined at 400°C), for the same deposited power (P=4W±5%)) are plotted in Fig. 3. In the fluidized bed reactor, the catalyst does not occupy the entire plasma zone, it is thus expected that filamentary microdischarges dominate while, for the fixed bed reactor, the complete packing of the reactor with alumina pellets results in the combination of filamentary and surface discharges. The breakdown of gas is expected to be lower in the presence of alumina powder and the electric field should be more intense at the contact points between pellets [14]. As a result, the applied voltage differs strongly between the two reactors to keep a constant power of 4 W. It is ~ 10 kV_{pk-pk} for the fixed bed and ~ 30 kV_{pk-pk} for the fluidized bed at constant frequency, 800Hz (Table 2).

3.2 Influence of the surface area of alumina

3.2.1 Chemical and physical properties of alumina

The alumina material was calcined at different temperatures from 400 to 800°C to vary the specific surface area and porous volume. The values obtained are gathered in Table 1. Prior to the reaction, all the solids were sieved in the range: 355-650 µm to eliminate the impact of the grain size on the reactivity, as shown in previous studies [19].

The total equivalent capacitance of the DBD (C_cell) and the effective capacitance (C_eff), corresponding to the capacitances in the plasma-off period and plasma-on period respectively, were determined from the Lissajous figures with the different alumina materials (Table 2). The value of C_cell is slightly higher for the fixed bed reactor compared to the fluidized bed, whatever the Al_2O_3 material. The reactor capacitances were approximately the same with or without material in the discharge zone, so the differences observed in C_cell values depend mainly on the reactor geometry, the packing with alumina having no significant impact on

C_cell. The effective capacitances are strongly higher for the fixed bed than for the fluidized bed, which can be explained by the expansion of the discharge across the gap [38].

Conversions of CH_4 and CO_2 are plotted as a function of the surface areas of alumina in figure 4. The data were collected after 30 minutes on stream since no significant modification of reactants transformation was observed within one hour under plasma. A different trend, occurring between the two reactors, was noticed. As soon as the surface area of alumina increases, CH_4 and CO_2 conversion decrease in the fixed bed reactor, while a significant increase for both CH_4 and CO_2 conversion is observed in the fluidized bed reactor. It is the first time, to our knowledge, that the influence of a material surface area is evidenced in the plasma-catalysis coupling. The results show undoubtedly that the combination of plasma and catalysis in a fluidized bed reactor can be efficient for methane and carbon dioxide conversion. Despite predominant gas phase reactions, these results highlight the importance of the surface reactivity of the material. No improvement is observed comparing the commercial γ-Al_2O_3 (S= 65 m^2 g^{-1}) to the material prepared in the laboratory (S= 260 m^2 g^{-1}). Differences in the synthesis procedure, which would induce different surface properties in terms of number of surface -OH groups per surface unit, would explain this result.

It is expected that in the fixed bed reactor, the reaction proceeds mainly at the contact point of the catalyst where the electric field is stronger but in a very limited reactional volume. Consequently, the porosity of the oxide is rapidly blocked by the deposition of heavy products such as C3 aldehydes and C5 ketones, detected after reaction by pyrolysis coupled with mass spectrometry. In a fixed bed reactor, the decrease of CH_4 and CO_2 conversions using porous materials such as zeolite was reported by Jiang et al. [39]. Inversely, in the fluidized bed reactor, the reaction can proceed on the overall surface of the moving catalyst grains in the plasma zone, thus favoring CH_4 and CO_2 conversions. This results in an increase of the analyzed products: CO, H_2 and hydrocarbons (mainly C_2H_6) as shown in figure 5.

A mechanism can be proposed for plasma- γ-Al_2O_3 assisted reaction according to the results we obtained and based on the published paper of N.N. Gadzhieva [40] and Liu et al. [41], and is presented in figure 6. This reaction cannot be dissociated from reaction in homogeneous phase. The dissociative adsorption of CH_4 at the surface of alumina is expected to proceed under plasma, which depends on the concentration of surface OH groups. Since Alumina is a material with a strong dipolar character, it contains numerous OH groups and becomes easily charged [35]. Reactions at the surface of Al_2O_3 could be written according to Eqs. (6) - (9):

$$M^+[OH]^-... [HO]^-M^+ \rightarrow M^+ + H_2O + O^{2-} + \square + M^+ \quad (6)$$

$$CH_4 \rightarrow CH_3^{\bullet} + H^{\bullet} \text{ in gas phase (under plasma discharge)} \quad (7)$$

$$O^{2-} + \square + CH_3 \rightarrow O\text{-}CH_3 \quad (8)$$

$$O\text{-}CH_3 \rightarrow CO_{ads} + 3/2\ H_2 \quad (9)$$

With $\square$ being an active site

The energy Efficiency (EE) is the highest using the fluidized bed reactor with the alumina possessing the highest surface area (Fig. 7). The trend of the energy efficiency is similar to the reactant conversions one, which is coherent since the reactions were performed at the same specific input energy (6 kJ L^{-1}) and both CH_4 and CO_2 conversions were favored using a fluidized bed reactor. The energy efficiencies were 0.07 and 0.14 mmol kJ^{-1} for the fixed bed and fluidized bed, respectively.

3.2.2 Structural and textural characterization of alumina materials before and after reaction under plasma

TGA analysis of the Al_2O_3 materials were performed after one hour of reaction under plasma for both reactors (Fig. 8). A continuous weight loss proceeds from low temperatures (T<100°C) to 600°C. It comes from the desorption of products, which were condensed into the porosity of alumina during the reaction under plasma. The yellowish color of the plasma treated samples

confirms the presence of organic compounds at the surface of alumina, except for the commercial Al_2O_3 (surface area 65 m^2 g^{-1}) after treatment in the fixed bed reactor. Moreover the presence of carbon deposit by methane cracking under plasma cannot be excluded, it would be removed at the highest temperature. The total weight loss is particularly significant (closed to 20%) for the alumina with the highest surface areas (301 and 312 m^2 g^{-1}) with the fluidized bed. It is in accordance with the carbon balance (Fig. 5d), which is the lowest for alumina with the highest surface area. The adsorption of heavy compounds at the surface of alumina would depend on the accessible surface. Indeed, it is expected that these products, formed in the plasma gas phase, are deposited in the porosity of alumina. However this effect depends on the catalyst pore size. According to Bogaerts et al. [42, 43], from a modeling investigation, plasma can only penetrate in pores larger than 50 nm and the alumina synthesized in this study possess pores from 4 to 8 nm (Table 1). Considering that their calculations were based on a glow mode, which differs strongly from the DBD plasma used in the present work, it would explain our results. In fact, when comparing the two reactors, no significant differences in terms of weight loss are observed for the alumina γAl_2O_3-600 and γAl_2O_3-800 while significant differences are obtained for γAl_2O_3-400 and particularly for the commercial γAl_2O_3. If we consider that the surface reaction proceeds only at contact point of grains in the fixed bed reactor, the low weight loss is due to the low accessible surface for products deposition. Contrarily, as soon as the alumina particles are fluidized, the product condensation proceeds on the entire accessible surface and possibly into the porosity of the commercial alumina which is significantly larger than the porosity of alumina synthesized in the laboratory.

The measurement of surface area after reaction (Table 1) reveals a significant loss for the meso-macro alumina materials synthesized in the laboratory, which is more intense for the fluidized bed than for the fixed bed. The exposition of the entire surface area of the material in the fluidized bed reactor, while localized at the contact point in the fixed bed reactor, would explain

these observations. Note that the value of pore size after reaction do not take into account organic compounds adsorbed during reaction, since the measurements require a thermal treatment under reduce pressure, leading to products elimination.

4. Conclusion

The transformation of a mixture of methane and carbon dioxide under plasma discharge in the presence of alumina was investigated in fluidized and static bed reactors.

Methane and carbon dioxide conversions depend on the surface area, a significant increase being obtained with alumina of large surface area in the fluidized bed reactor. CH_4 conversion increases from 8.5 to 12.1 % for S=260 and 312 m^2 g^{-1}, respectively and the CO_2 conversion from 3.4 to 6.2 % for a deposited power of 4 W, in an excess of CO_2. An opposite trend is obtained between fluidized and fixed bed reactors. This effect is to the limited accessible catalyst surface in the fixed bed, at the contact point of grains, were the electric field is the most intense. In the fluidized bed, the overall grain surface is involved in the plasma-catalytic reaction and higher conversions to products such as CO and ethane are obtained. Reactions at the surface of Al_2O_3 under plasma discharge are proposed. Condensation of organic products into the porosity of alumina was evidenced whatever the surface area of alumina. The deposition of organic products is favored in the alumina of largest porosity (23 nm), in fluidized mode. The stacking of grains in the fixed bed mode limits this effect.

To conclude the use of a plasma fluidized bed might be considered as an attractive process to enhance performances of plasma-catalysis coupling. It opens new routes for the investigation of a wide variety of reactions thermodynamically unfavorable.

Acknowledgements

The authors grateful acknowledge the ANR for the financial support of the PRC program VALCO2PLAS and the financial support from the European Union (ERDF) and "Région Nouvelle Aquitaine".

References

[1] E. Ruckenstein, H.Y. Wang, J. Catal. 205 (2002) 289-293

[2] M. Usman, W.M.A. Wan Daud, H. F. Abbas, Renew. Sust. Energy Rev. 45 (2015) 710-744

[3] A.J. Zhang, A.M. Zhu, J. Guo, Y. Xu, C. Shi, Chem. Eng. J. 156 (2010) 601–606

[4] M. Kraus, W. Egli, K. Haffner, B. Eliasson, U. Kogelschatz, A. Wokaun, Phys. Chem. Chem. Phys. 4 (2002) 668–675

[5] X. Tao, M. Bai, X. Li, H. Long, S. Shang, Y. Yin, X. Dai, Prog. Energy Combust. Sci. 37 (2011) 113–124

[6] B. Wang B, G. Xu (2003) J Nat Gas Chem 12 (2003) 178–182

[7] B. Fidalgo, J.A. Menéndez, Fuel processing technology, 95 (2012) 55-61

[8] X. Tu, J.C. Whitehead, Int. J. Hydrogen Energy, 39 (2014) 9658-9669

[9] N. Rueangjitt, T. Sreethawong, S. Chavadej, H. Sekiguchic, Chem. Eng. J. 155 (2009) 874-880

[10] M. Kraus, B. Eliasson, U. Kogelschatz, A. Wokaun, Phys. Chem.Chem. Phys. 3 (2001) 294-300

[11] B. Eliasson W. Egli, U. Kogelschatz Pure Appl Chem 66(6) (1994) 1275–1286

[12] H. Puliyalil, D.L. Jurkovic, V.D. Dasireddy, B. Likozar, RSC Adv. 8 (2018) 27481-27508

[13] E.C. Neyts, K. Ostrikov, M. K. Sunkara, A. Bogaerts, Chem. Rev. 115 (2015) 13408-13446

[14] X. Tu, H.J. Gallon, M. V. Twigg, P. A. Gorry, J.C. Whitehead, J.Phys. D: Appl. Phys. 44 (2011) 274007-274017

[15] T. Jiang, Y. Li, C.J. Liu, G.H. Xu, B. Eliasson, B. Xue, Catal. Today, 72 (2002) 229-235

[16] H.J. Gallon, X. Tu, J.C. Whitehead, Plasma Process and Polymer, 9 (2012) 90-97

[17] X. Tu, H.J. Gallon, M. V. Twigg, P. A. Gorry, J.C. Whitehead, J.Phys. D: Appl. Phys. 44 (2011) 274007-274017

[18] P. Kasinathan, S. Park, W.C. Choi, Y.K. Hwang, J.S. Chang, Y.K. Park, Plasma Chem. Plasma process. 34 (2014) 1317-1330

[19] N. Bouchoul, J.M. Tatibouët, E. Fourré, C. Batiot-Dupeyrat, Plasma Chem. and Plasma Process., 39 (2019) 713-727

[20] R. Bartolomeu, M. Foix, A. Fernandes, M. Tatoulian, M.F. Ribeiro, C. Henriques, P. da Costa, Catal. Today, 176 (2011) 234-238

[21] G. Hee Kim, S. D. Kim, S. H. Park, Chem. Eng. Process. 48 (2009) 1135-1139

[22] G. Chen, S. Chen, M. Zhou, W. Feng, W. Gu, S. Yang, J. Phys. D: Appl. Phys. 39 (2006) 5211-5215

[23] G. Chen, S. Chen, W. Feng, W. Chen, S. Yang, Appl. Surf. Sci. 254 (2008) 3915-3920

[24] Q. Wang, Y. Cheng, Y. Jin, Catal. Today, 148 (2009) 275-282

[25] W. Wang, H.H. Kim, K. Van Laer, A. Bogaerts, Chem. Eng. J. 334 (2018) 2467-2479

[26] N. Bouchoul, E. Fourré, A. Duarte, N. Tanchoux, C. Louste, C. Batiot-Dupeyrat, Catal. Today, in press 2020, doi.org/10.1016/j.cattod.2020.06.058

[27] S. Ergun, Chem. Engrg. Progress, 48, No. 2, (1952) 89–94

[28] Wen, C. Y. and Yu, Y. H., Chem. Engrg. Progress Symp. Series, Vol. 62 (1966) 100–111

[29] R.P. Currier, M. Trkula, H.R. Snyder, The plasma fluidized bed, a report, DOI:10.2172/758321

[30] Z-Y. Yuan, T-Z. Ren, A. Vantomme, B-L. Su, Chem. Mater 16 (2004) 5096-5106

[31] N. Rueangjitt, T. Sreethawong, S. Chavadej, H. Sekiguchi, Plasma Chem. Plasma Process (2011) 31, 517-534

[32] Nozaki T, Miyazaki Y, Unno Yand Okazaki K. (2001) Journal of Physics D: Applied Physics 34, 3383-90

[33] V. Goujard, J.M. Tatibouët, C. Batiot-Dupeyrat, Appl. Catal. A : Gen, 353 (2009) 228-235

[34] J. Sentek, K. Krawczyk, M. Mlotek, M. Kalczwska, T. Kroker, T. Kolb, A. Schenk, K.H. Gericke, K. S. Szalowski, Appl. Catal. B: Env. 94 (2010) 19-26

[35] N.B. Uner, E. Thimsem, Aiche J. 2020,;66e16948

[36] E.Y. Mora, A. Sarmiento, E. Vera, J. Phys.: Conf. series 687 (2016) 012020

[37] A. H. Khoja, M. Tahir, N. A. S. Amin, Energy Conv. And Management, 144 (2017) 262-274

[38] S. Jo, D. H. Lee, W. S. Kang, Y.H. Song, Physics of plasmas, 20 (2013)123507

[39] Y. Jiang, Y. Li, C.J. Liu, G.H. Xu, B. Eliasson, B. Xue, Catal Today 72 (2002) 229–235

[40] N.N. Gadzhieva, High Energy Chemistry, 37 (2003) 38-43

[41] C. Liu, A. Marafee, R. Mallinson, L. Lobban, Appl. Catal. A: gen 164 (1997) 21-33

[42] Y.R. Zhang, K.Van Laer, E. C. Neyts, A. Bogaerts, Appl. Catal. B: Env 185 (2016) 56-67

[43] Q.Z. Zhang, A. Bogaerts, Plasma Sources Sci. Technol. 27 (2018) 35009-35019

Table 1: Properties of the gamma alumina: surface area and pore volume before and after reaction under plasma (1 hour, grain size: 355-650 µm, P=4 W, total flow: 40 mL min^{-1}, CO_2/CH_4=2, He: 75%)

Oxide	S BET (m^2 g^{-1})			Pore size (Å)		
	Before plasma	After plasma		Before plasma	After plasma	
		Fixed bed	Fluidized bed		Fixed bed	Fluidized bed
γAl_2O_3-AA	65	64	64	230	230	230
γAl_2O_3-400	312	305	298	64	64	64
γAl_2O_3-600	301	282	275	76	75	76
γAl_2O_3-800	260	183	165	41	42	41

Table 2: Characteristics of the discharge for the two plasma reactors: fixed and fluidized bed at a constant deposited power: P=4 W, grain size: 355-650 µm, total flow: 40 mL min^{-1}, CO_2/CH_4=2, He: 75%

Catalyst bed	U peak-peak (kV)		C_cell (pF)		C_eff (pF)	
	Fixed	Fluidized	Fixed	Fluidized	Fixed	Fluidized
γAl_2O_3-AA	10.4	30.5	1.3	0.9	32.9	3.9
γAl_2O_3- 400	10.2	30.8	1.2	0.8	33.7	3.7
γAl_2O_3- 600	10.2	30.6	1.4	1.0	32.7	4.1
γAl_2O_3-800	10.5	30.4	1.6	0.9	31.2	3.8

Figure 1: Reactor scheme a) Fixed bed reactor, b) fluidized bed reactor

a)

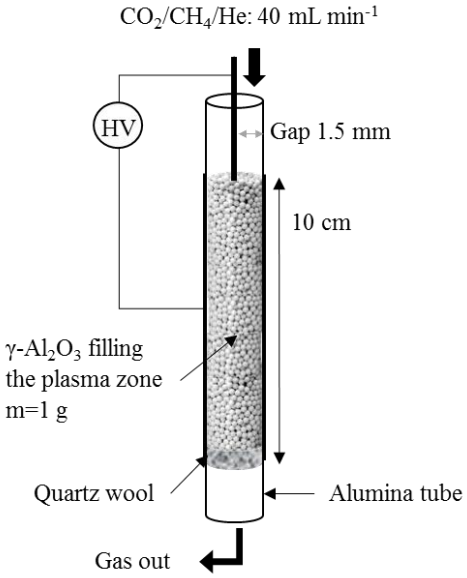

b)

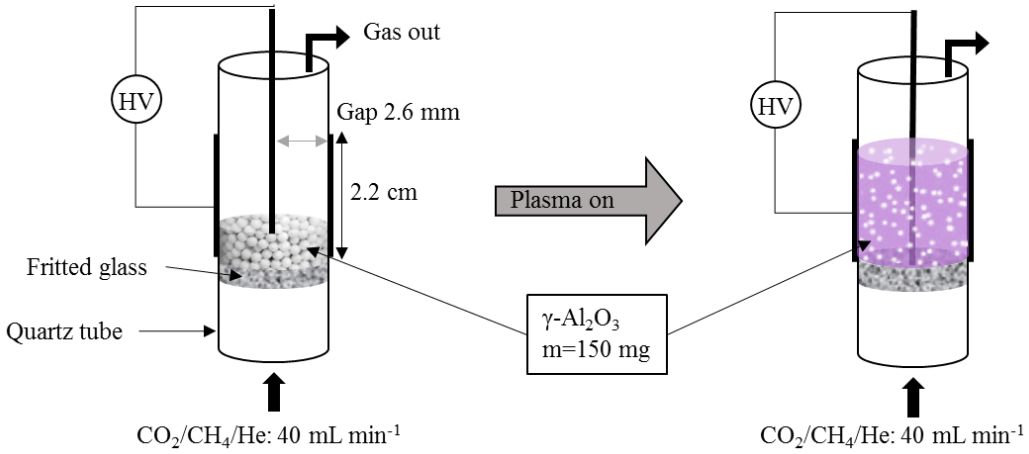

b1: Without plasma b2: With plasma P=4 W

Figure 2: CO_2 and CH_4 conversion, yield into CO, H_2 and hydrocarbons (mainly C_2H_6): influence of reactor geometry. P=4 W, total flow: 40 mL min^{-1}, CO_2/CH_4=2, He: 75% (data after 30 minutes on stream) ▒ fluidized bed, □ fixed bed

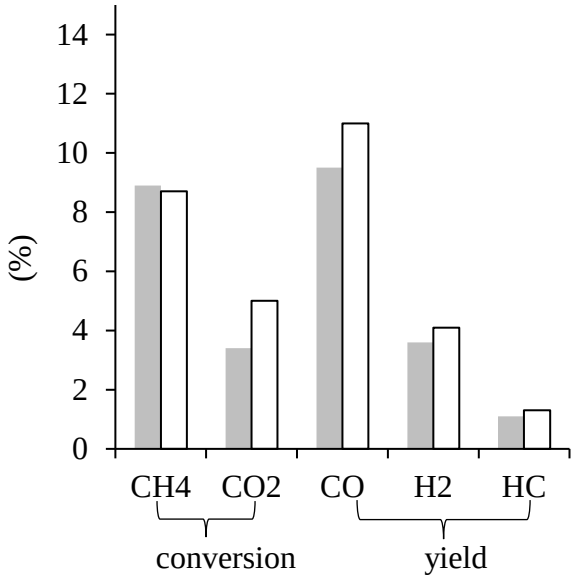

Figure 3: a) Lissajous figures of the CO_2/CH_4 DBD with alumina pellets for the fixed bed and fluidized bed reactor at a constant discharge power of 4 W (total flow: 40 mL min^{-1}, CO_2/CH_4=2, He: 75%), b) typical Lissajous figures, determination of C_cell and C_eff

a)

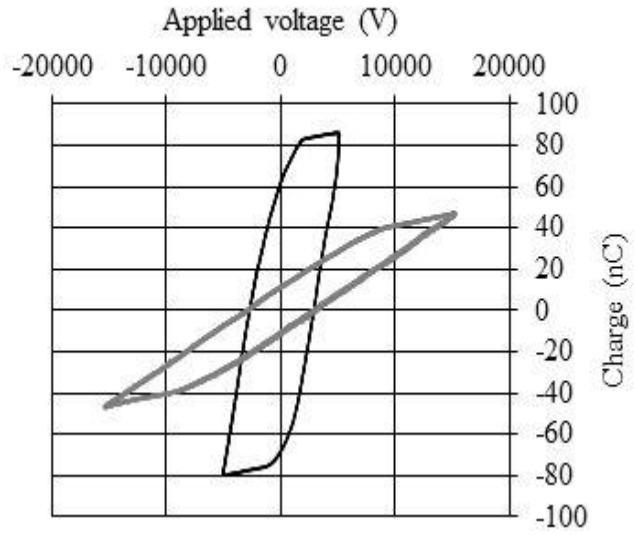

b)

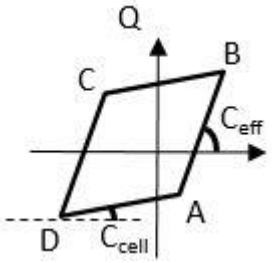

Figure 4: CO_2 and CH_4 conversion over gamma alumina: influence of surface area and reactor geometry. Grain size: 355-650 µm, P=4 W, total flow: 40 mL min^{-1}, CO_2/CH_4=2, He: 75% (data after 30 minutes on stream) ⟡ fluidized bed, + fixed bed

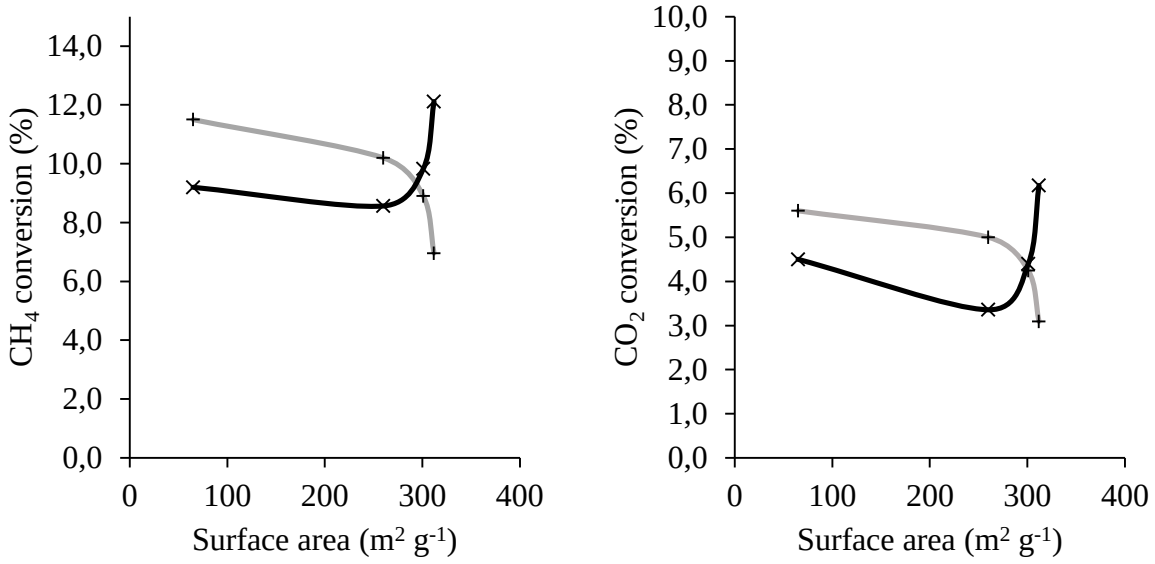

Figure 5: CO**,** H_2, hydrocarbon yield and carbon balance over gamma alumina: influence of surface area and reactor geometry. Grain size: 355-650 µm, P=4 W, total flow: 40 mL min^{-1}, CO_2/CH_4=2, He: 75%, (data after 30 minutes on stream)–x– fluidized bed, –+– fixed bed

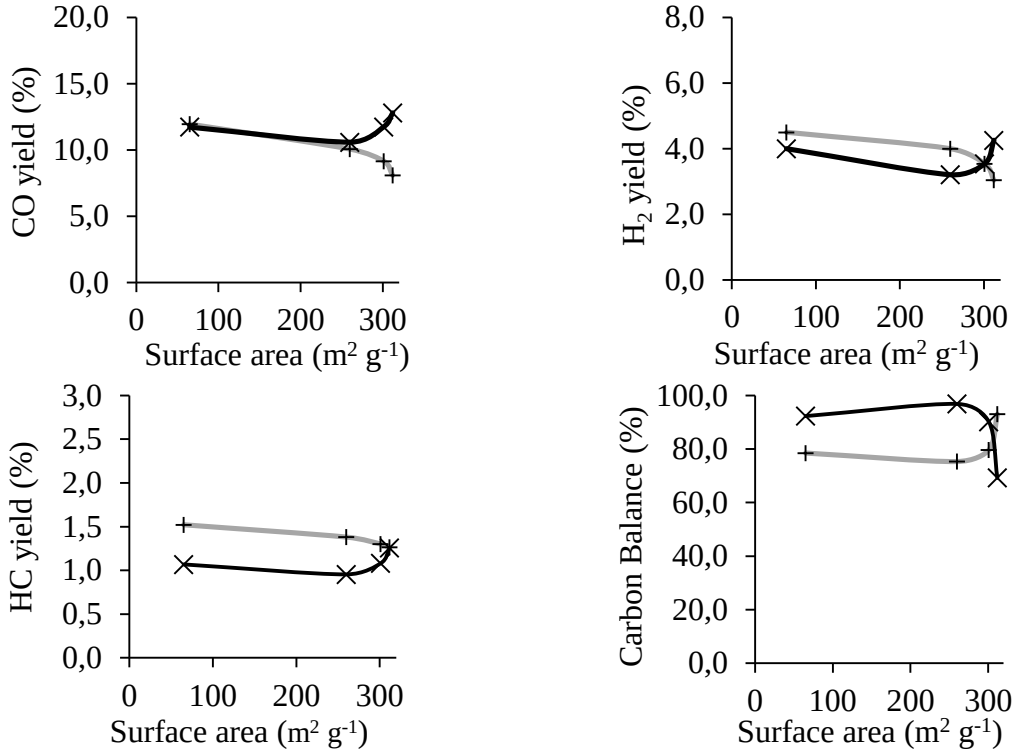

Figure 6: Schematic illustration of plasma discharge and reaction at the surface of γ-Al_2O_3 in fixed bed and fluidized bed reactor (not to scale)

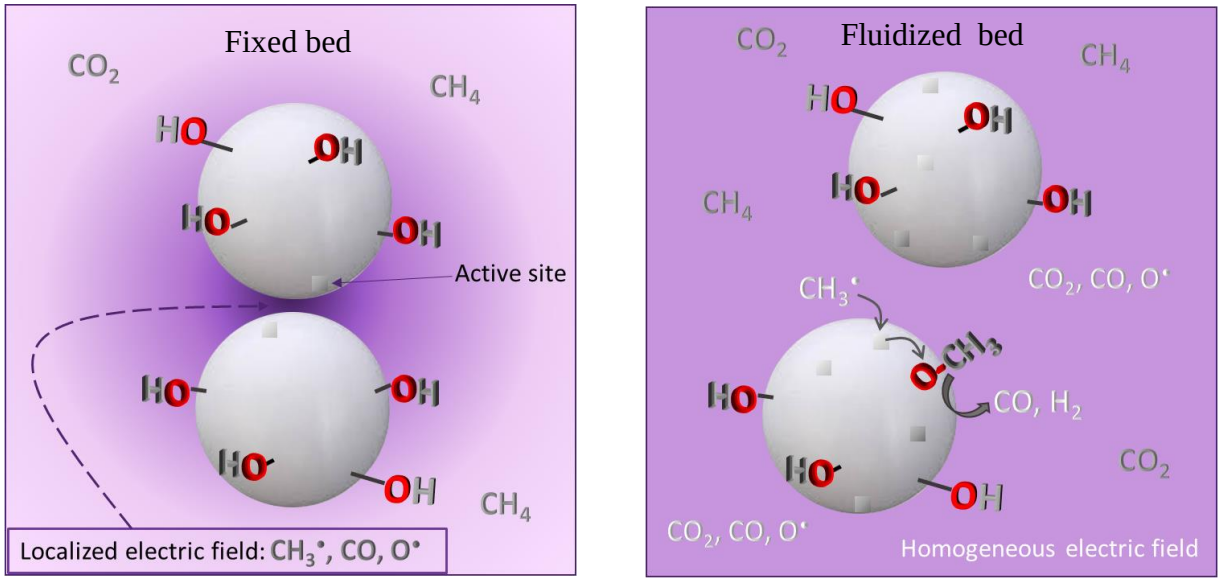

Figure 7: Effect of surface area of gamma alumina on Energy Efficiency for the two reactors geometry. Grain size: 355-650 µm, P=4 W, total flow: 40 mL min^{-1}, CO_2/CH_4=2, He: 75%, (data after 30 minutes on stream) ⊸ fluidized bed, ⊸ fixed bed

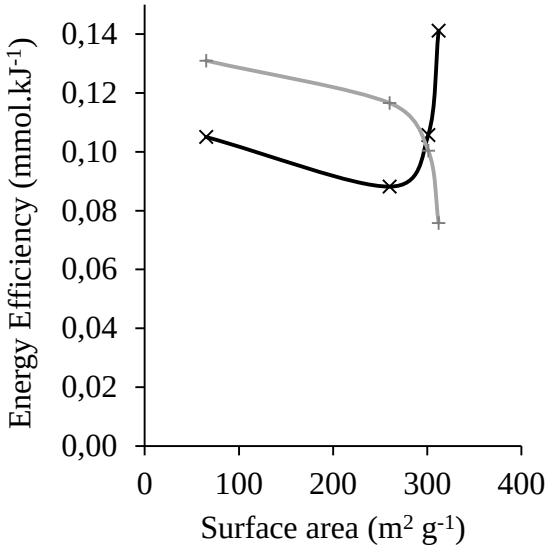

Figure 8: TGA analysis of alumina calcined at different temperatures, after reaction under plasma (60 minutes), grain size: 355-650 µm, P=4 W, total flow: 40 mL min^{-1}, CO_2/CH_4=2, He: 75%, fixed bed reactor, fluidized bed reactor